Dalton Transactions

Accepted Manuscript

ROYAL SOCIETY OF CHEMISTRY

www.rsc.org/dalton

Coinage Metal Complexes Supported by a "PN^3P" Scaffold.

Gyandshwar Kumar Rao, Serge I. Gorelsky, Ilia Korobkov, Darrin Richeson.*

Center for Catalysis Research and Innovation and Department of Chemistry and Biomolecular Sciences, University of Ottawa, Ottawa, Ontario, K1N 6N5

ABSTRACT

A series of monovalent group 11 complexes, [2,6-{Ph_2PNMe}$_2$(NC_5H_3)]CuBr **1**, [2,6-{Ph_2PNMe}$_2$(NC_5H_3)]CuOTf **2**, [2,6-{Ph_2PNMe}$_2$(NC_5H_3)]AgOTf **3**, and [2,6-{Ph_2PNMe}$_2$(NC_5H_3)]$(AuCl)_2$ **4**, supported by a neutral PN^3P ligand have been synthesized and characterized by multinuclear NMR and single crystal X-ray diffraction studies. The variation of the coordination properties were analyzed and electronic structure calculations have been carried out to provide insight on the bonding details in these complexes. The Cu(I) complexes displayed an unusual coordination geometry with a tridentate pincer ligand and an overall four coordinate trigonal pyramidal geometry. In contrast the Ag(I) analogue displayed a bidentate κ^2-P,P′ ligation leaving the pyridyl-N atom uncoordinated and yielding a pyramidalized trigonal planar geometry around Ag. The bimetallic Au(I) complex completed the series and displayed a monodentate P-bonded ligand and a linear coordination geometry.

Introduction

Pincer ligands provide the potential for a tridentate scaffold that is recognized as an effective means to modify and control the properties of metal complexes across the periodic table. They are usually anchored around a central aromatic backbone that is tethered to two Lewis base donor groups which are separated with different spacers. The most developed class of pincers are monoanionic with the central "pivot" site being deprotonated. There are also a number of neutral systems, often built around neutral pyridine-based frameworks with NNN, PNN and PNP donor arrays. The design and application of these species has been reviewed by several groups across the continuum of synthesis, small molecule reactivity and catalysis.[1–13]

Our interest in pincer ligands began with the application of bis(imino)pyridine scaffolds (an NNN framework) to investigate fundamental bonding issues in main group metal and Ag(I) complexes and with their ability to provide the appropriate ligand field and coordination geometry to prepare monometallic single molecule magnets.[14–20] With the idea of extending this chemistry and developing new directions we were interested in examining the neutral ligands derived from the N,N'-bis(diphenylphosphino)-2,6-diaminopyridine (**A**) architecture and their application as pincer ligands.

N,N'-bis(diphenylphosphino)-2,6-diaminopyridine (**A**) was first introduced in 1987 with the characterization of neutral carbonyl compounds of group 6 and as complexes of divalent MCl_2 (M= Ni, Pd, Pt) species.[21,22] These researchers also reported an In(III) compound, [2,6-$\{Ph_2PNH\}_2(NC_5H_3)$]$InCl_3$ displaying a meridionally coordinated ligand to yield a pseudooctahedral complex.[23] This ligand framework was significantly expanded by the Kirchner group with variation to both the P-Ph groups and the N-H moieties.[24–30] In particular we were interested in exploring the use of the N-Me ligand **B** as this modification would remove a

reactive site for deprotonation, introduce a steric load to the ligand and may provide stronger electron donation to a coordinated metal center.[24–26,31,32]

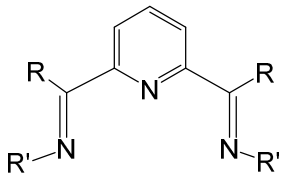

bis(imino)pyridine

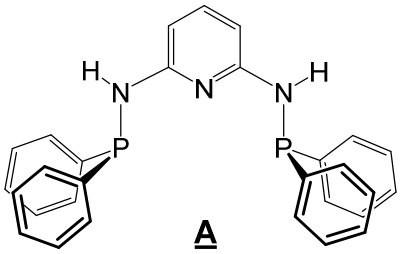

A

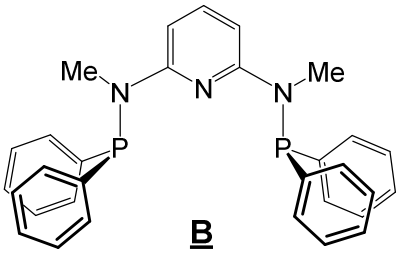

B

The literature for this ligand family ("PN^3P") has been recently reviewed.[5] As with pincer complexes in general,[33] the application of N,N'-bis(diphenylphosphino)-2,6-diaminopyridine ligand family with the coinage metals has been largely unexplored.[34,35] In fact, there are no reported complexes of these ligands with Ag and, to our knowledge, only one example for Au.[35] Herein we report the group 11 complexes of N,N'-bis(diphenylphosphino)-2,6-di(methylamino)pyridine (**B**). The Cu-Br and CuOTf (OTf = OSO_2CF_3) complexes display unique molecular structures and their bonding features were analyzed by computation. Furthermore, the first Ag complex of this ligand family is reported and structurally and computationally investigated. The series was completed with the elucidation of the structure for the monovalent Au compound.

Results and Discussion

Reaction of soluble N,N′-bis(diphenylphosphino)-2,6-di(methylamino)pyridine ligand (**B**) with a Cu(I) starting material, $CuBr(SMe_2)$, led to the formation of a light green species **1** (82%) (Scheme 1). The multinuclear NMR spectroscopy analysis of this species was consistent with reported complexes of this ligand as well as complexes supported by ligand **A**.[24,30] These

features, in combination with high-resolution mass spectrometry and microanalysis, were consistent with the formation of the complex, [2,6-{Ph_2PNMe}$_2$(NC_5H_3)]CuBr (**1**). Fortunately X-ray quality crystals of **1** could be reproducibly obtained and used to confirm the proposed identity and structural features for **1** (Figure 1).

SCHEME 1.

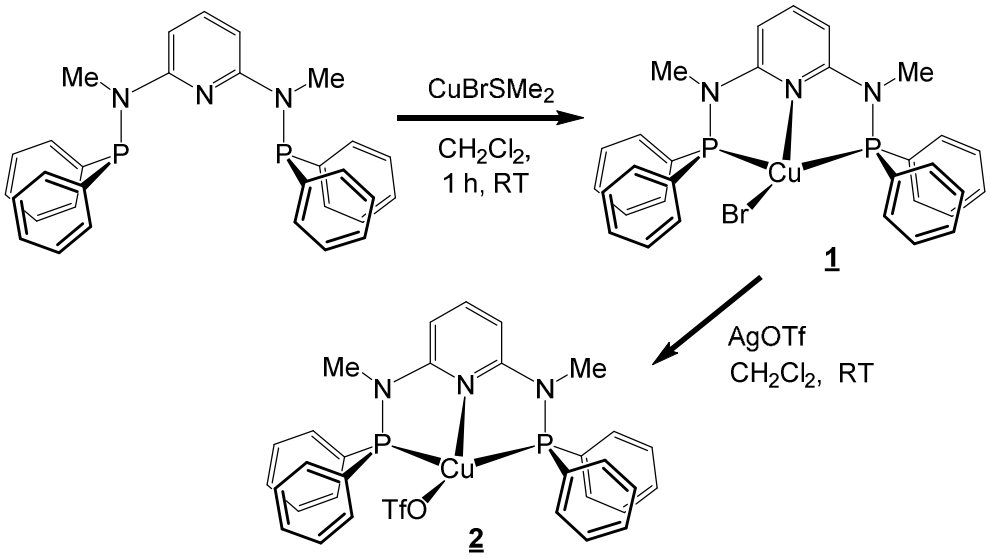

Complex **1** displayed a four-coordinate Cu center with the pincer ligand coordinated in a κ^3(P,N,P′) fashion and with symmetrical Cu-P distances (2.2245(4) and 2.2386(4) Å) and a Cu(1)-N(1) distance of 2.1230(11) Å. The coordination geometry is best described as distorted trigonal pyramid with the pyridyl-N center residing in the apical position and the base defined by P(1), P(2) and Br(1) (sum of basal angles = 360°). Using the τ_4 index, compound **1** gives a value of 0.78 which is more consistent with trigonal pyramidal rather than seesaw geometry.[36] The d^{10} ions of the coinage metals are known to demonstrate variable coordination geometry with Cu(I) predominantly found as tetrahedral species, thus making **1** an unusual coordination geometry.[37]

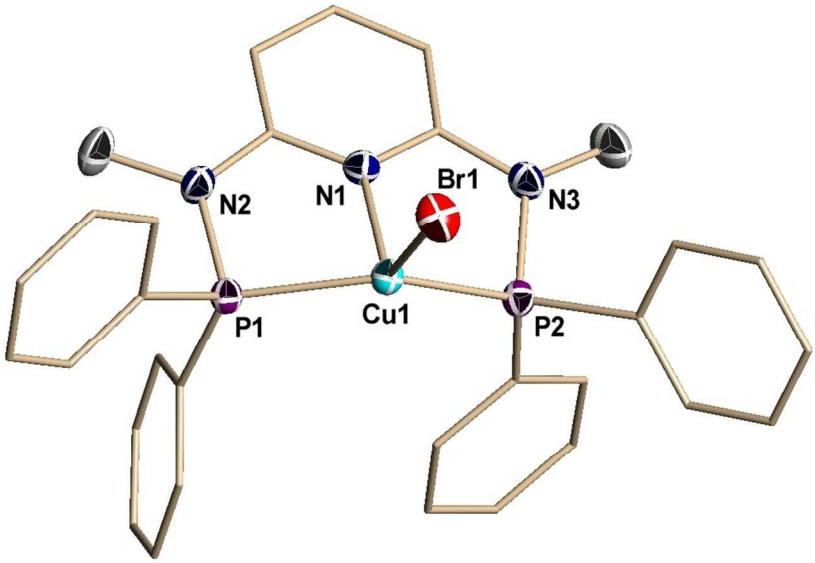

Figure 1. Structural representation of compound **1**. Hydrogen atoms and thermal ellipsoids of the ligand carbon atoms are omitted for clarity. Full structural information can be found in the Supporting Information. Selected bond lengths (Å) and bond angles (deg): Cu(1)-N(1) 2.1230(11), Cu(1)-P(1) 2.2245(4), Cu(1)-P(2) 2.2386(4), Cu(1)-Br(1) 2.3797(2), P(1)-N(2) 1.7207(12), P(2)-N(3) 1.7295(12), N(1)-Cu(1)-P(1) 80.69(3), N(1)-Cu(1)-P(2) 79.43(3), P(1)-Cu(1)-P(2) 134.835(14), N(1)-Cu(1)-Br(1) 115.17(3), P(1)-Cu(1)-Br(1) 115.413(12), P(2)-Cu(1)-Br(1) 109.736(11).

While related potential pincer ligands have been employed with Cu(I) (see **C**-**G**) , the structure obtained for **1** is significantly different from all of these reported species. For example, application of the analogous PN^3P ligand with NH rather than NMe led to isolation of tetrahedral Cu compounds **C** or **D**, depending on reaction stoichiometry.[35] These species exhibit preferential ligand coordination to a single metal center in a chelating bidentate fashion rather than as a pincer ligand. In the case of the bimetallic species **D**, the pendant phosphorus center from

another ligand bonds to the alternate Cu(I) center. Compounds derived from **E** have been the most thoroughly reported to date.[38–40] In this case the ligand is formally related by replacement of the NR spacer with a CH_2 group. Complex **E**, with a single ^{31}P NMR resonance at δ 46.2 (acetone-d_6), displayed a distorted trigonal planar coordination geometry with slightly longer Cu-P and Cu-Br distances (Cu-P, 2.3150(5), 2.3104(5)Å; Cu-Br, 2.4376(3) Å) than observed in **1**. The Cu-N_{py} distance in **E** with a value of 2.8938(17) Å was considered to be well-removed from bonding to Cu(I). It was possible to provoke coordination of the pyridyl group to the Cu center, as in **F**, by either halide abstraction to yield a cationic complex or by deprotonation of the CH_2 linker with subsequent halide loss. These cationic compounds exhibit typical Cu-N_{py} distances of 2.091-2.157Å. The cationic Cu(I) complex formed from a 2,6-bis(2-phosphaethenyl)pyridine ligand (**G**) adopted a distorted seesaw (P-Cu-P axial) geometry defined by a κ^3(P,N,P′) ligand and a coordinated MeCN. The Cu-N_{py} (2.071(4)Å), Cu-$NCCH_3$ (1.939(4)Å), and Cu-P (2.313(1), 2.303(1)Å) lengths are typical for such single bonds.[41] A diphosphinine analogue of terpy functioned as a pincer ligand to generate compound **H** which displayed bond distances similar to those observed for **1**.[42] Specifically, the average Cu-P, Cu-N and Cu-Br distances were 2.27, 2.09, and 2.33Å, respectively. However, unlike the coordination environment in **1**, **H** was characterized as distorted tetrahedral or "butterfly". The differences observed between complex **1** and complexes **C** and **D** is particularly instructive and may be attributed to the fact that ligand **B** is a stronger electron donor than **A** and hence leads to stronger coordination and more stable complexes.[24]

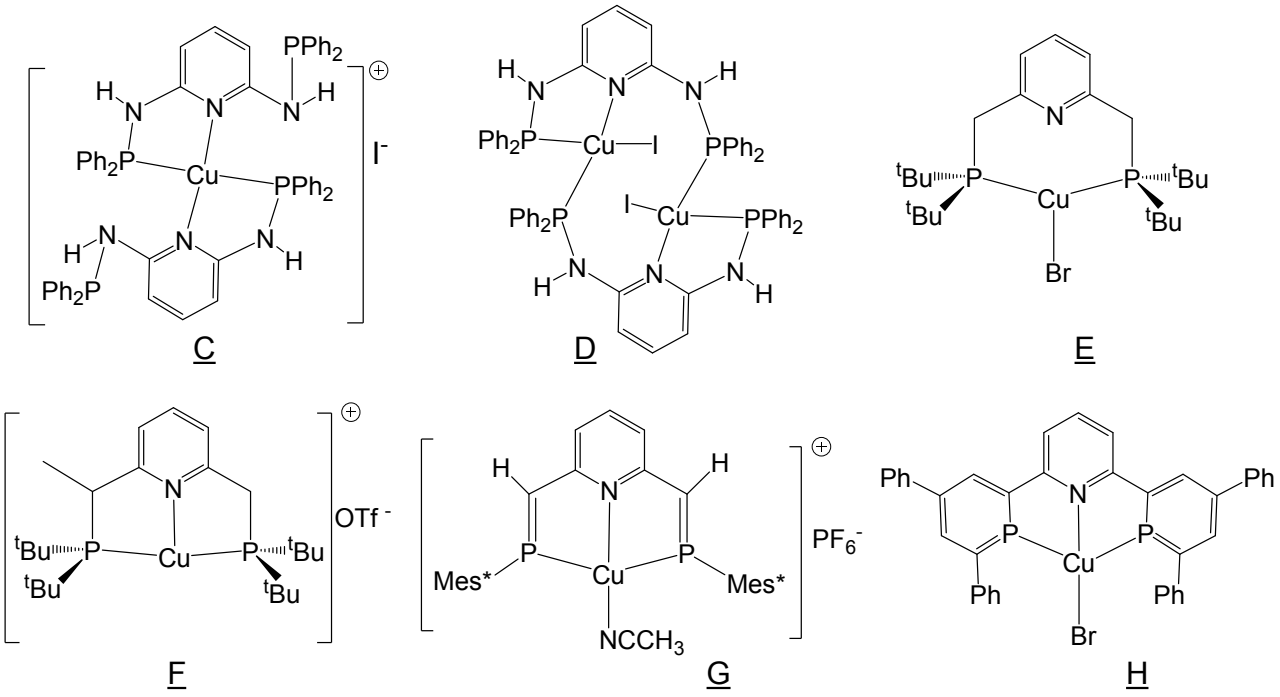

As shown in Scheme 1, complex **1** reacted cleanly with AgOTf in dichloromethane solution to eliminate AgBr and yield the soluble Cu(I) complex, **2**. The NMR spectra (^{1}H, ^{13}C and ^{31}P) of complex **2** were similar to compound **1** and suggest that this new compound is consistent with the proposed constitution. Definitive confirmation of the molecular structure was obtained through single crystal X-ray analysis (Figure 2).

The structure of complex **2** displays close contacts with the three donor atoms of the pincer ligand, P1, P2 and N2, as well as with one of the OTf oxygen atoms, O1. With the P1, P2 and O1 residing in a plane (Σ angles = 359.4º) and the N_{py} approximately perpendicular to this plane, a trigonal pyramidal geometry, like compound **1**, provides the best structural description for **2**. The Cu-N_{py} bond length at 2.0574(12)Å is slightly shorter than that of the bromide analogue **1** suggesting a higher effective charge on Cu and weaker anion interaction with the metal. The Cu-P distances in **2** are the same as in **1** but the shift of the Cu toward the N_{py} apex results in an increase in the P-Cu-P angle to 142.8º. At first glance there may appear to be a structural

similarity between complex **2** and compound **F.** However, **F** displayed a non-interacting OTf anion and, in contrast to **2**, the T-shaped coordination geometry of **F** exhibited a nearly linear P-Cu-P angle (171.82(10)º), slightly shorter Cu-P distances (2.213Å) but a longer Cu-N_{py} distance of 2.109(5)Å than **2**.[38]

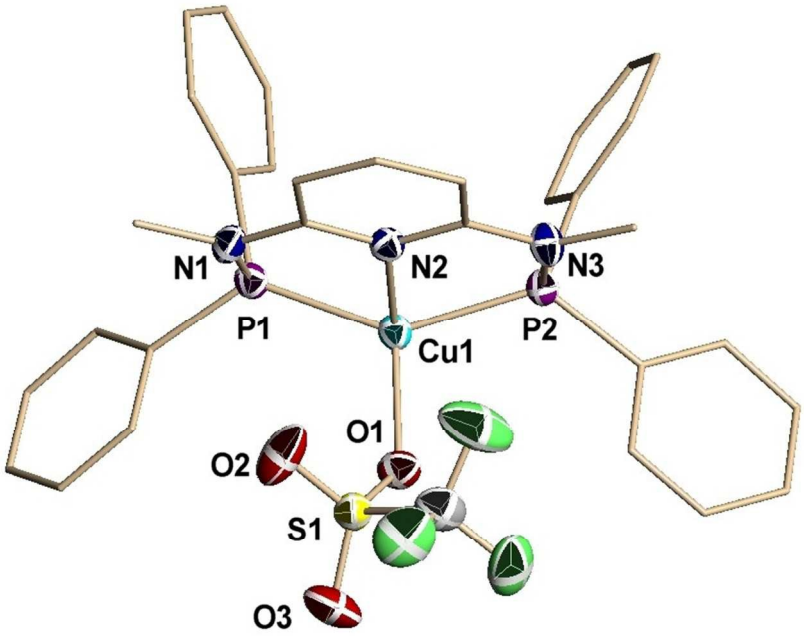

Figure 2. Structural representation of compound **2**. Hydrogen atoms and thermal ellipsoids of the ligand carbon atoms are omitted for clarity. Full structural information can be found in the Supporting Information. Selected bond lengths (Å) and bond angles (deg): Cu(1)-N(2) 2.0574(12), Cu(1)-O(1) 2.1620(11), Cu(1)-P(2) 2.2264(4), Cu(1)-P(1) 2.2301(4), P(1)-N(1) 1.7154(14), P(2)-N(3) 1.7205(13), N(2)-Cu(1)-O(1) 104.97(5), N(2)-Cu(1)-P(2) 82.72(4), O(1)-Cu(1)-P(2) 103.86(3), N(2)-Cu(1)-P(1) 81.53(3), O(1)-Cu(1)-P(1) 112.74(3), P(2)-Cu(1)-P(1) 142.757(16)

Given the unique structural features of **1** and **2** we sought a more detailed analysis of the bonding in these species through DFT optimization (B3LYP functional, TZVP basis set) and analysis. In the case of **1**, the electronic interaction energy between the [2,6-

{Ph_2PNMe}$_2$(NC_5H_3)]Cu and Br fragments was determined to be -104 kcal/mol with a Mayer bond order of 0.8, consistent with a σ interaction between these two components. A significant level of charge transfer from the bromine center to the LCu fragment of 0.46 electrons was also obtained from this analysis.

Turning attention to the bonding between the PN^3P pincer ligand and the Cu cation center in the [2,6-{Ph_2PNMe}$_2$(NC_5H_3)]Cu fragment of complex **1**, the overall electronic interaction energy was determined to be -130.6 kcal/mol with a total bond order of 1.9 corresponding to donation of 0.97 electrons. These values are consistent with the observed bond distances and with the ligand donating enough electron density to effectively quench the charge on the monovalent Cu center. A closer look at the bonding interactions revealed that the ligand donation is dominated by contributions from the two P centers and comes predominantly from six highest occupied fragment orbitals (HOFO's, Figure 3). With a filled set of *d*-orbitals, the major acceptor orbital on the Cu(I) center is the empty 4s orbital (LUFO) which changes its orbital occupancy by 35.5% reflecting donation from the ligand. There is a significant but smaller amount of charge transfer through σ-donation to Cu 4p (LUFO+2 change in orbital occupancy by 12.3%) that is orientated to accept donation from the two phosphine groups. The relative contributions to the bond order from each of the Cu-P interactions was determined to be 0.77 while that from the Cu-N_{py} donation was only 0.21, clearly demonstrating the dominance of the Cu-P bonding in **1**.

It is useful to examine the specific ligand donor orbitals and these fragment orbitals (HOFOs) are displayed in Figure 3 along with the percent orbital occupancy change from donation to Cu. A general feature of these HOFOs is the primary role of the P-centered electrons. Unique among the six donors, HOFO and HOFO-2 have an antisymmetric combination of the lone electron pairs on the two P centers making these two orbitals appropriate for σ-donation into the 4p on

the Cu(I) center. The remaining four HOFOs have symmetries to donate to a Cu 4s orbital but with some subtle features of interaction. Donation from the HOFO-1 involves all three lone electron pairs on the ligand with an in-phase/symmetric combination for the phosphine groups but opposite phase from the N_{py}. As a result HOFO-1 experiences a combination of P-bonding and N-antibonding interactions with the Cu 4s orbital. Donation from the HOFO-6 orbital is predominantly lone pair on N_{py} but this σ-donation to the 4s Cu orbital is a very small (3.5%) bonding contribution. The two remaining donors, HOFO-12 and HOFO-13, involve the lone electron pairs on the phosphine groups along with contribution from the polarized π-system of the pyridyl group that is centered on the N_{py} center. These orbitals form a σ bonding interaction between the pincer ligand and the Cu 4s orbital.

A similar DFT computational analysis of **2** (i.e. B3LYP/TZVP) allows for comparison with **1**. Consistent with a reduction in the interaction and covalency between the [2,6-$\{Ph_2PNMe\}_2(NC_5H_3)$]Cu and the OTf fragments was the lower computed electronic interaction energy of -82.9kcal/mole, a reduced bond order of 0.35 and the smaller degree of electron transfer from the OTf^- to LCu^+ of only 0.2 electrons.

Small but significant changes were observed in the electronic interactions between the pincer ligand and the Cu center. An electronic energy of -134.3kcal/mol was obtained for the ligand/Cu(I) interaction of **2** which corresponded to an overall bond order between these fragments of 1.98. The ligand donates about 1.2 electrons to the Cu(I) center in **2** with about 0.2 electron back donation from the metal to the PN^3P ligand to yield a net donation of only 1 electron from the ligand. All of these parameters point to a stronger metal ligand interaction for **2** relative to **1** that is consistent with expectations. As with **1**, the Cu-based acceptor orbitals are the 4s orbital (LUFO) that has a change in orbital occupancy of 36.5% and the 4p orbital (LUFO+3)

that is oriented toward the two P donor centers and changes its occupancy by 14.2% through donation predominantly from the ligand donor orbitals HOFO and HOFO-2 (*vide infra*).

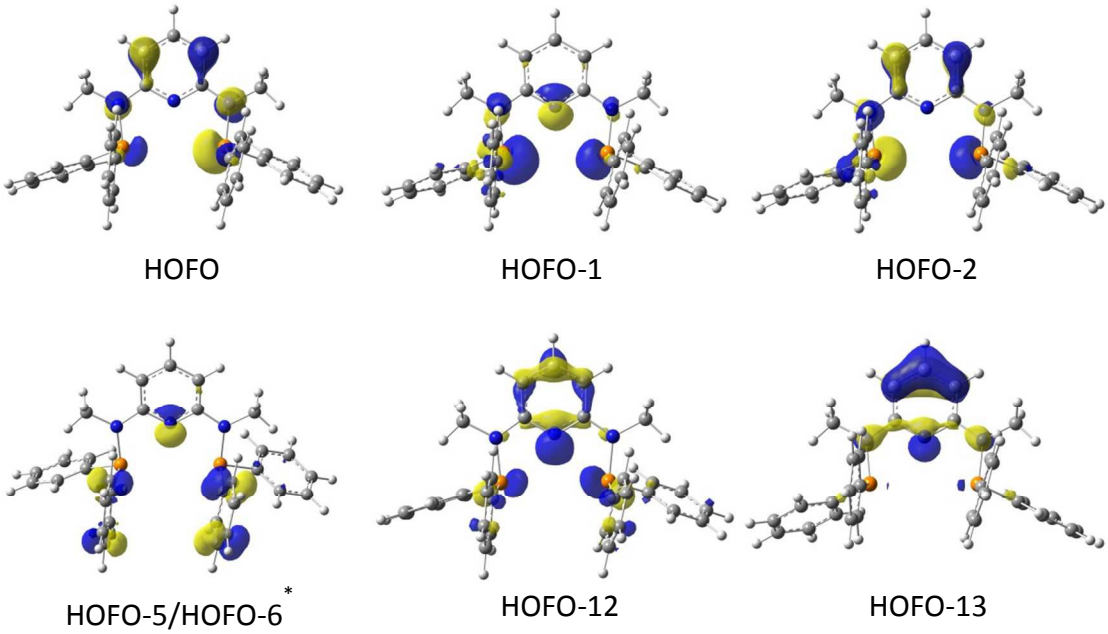

cmpd	HOFO % change	HOFO-1 % change	HOFO-2 % change	HOFO-5/ HOFO-6* % change	HOFO-12 % change	HOFO-13 % change
1	4.9	17.8	6.5	3.5	8.0	5.7
2	6.7	17.3	6.1	2.3	8.0	5.4
3	6.3	15.4	5.2	1.3	4.6	5.2

Figure 3. Isosurface images of the six donor ligand fragment orbitals (highest occupied fragment orbital = HOFO) that are the major contributors to bonding in compounds **1-3.** The specific orbitals shown are for compound **2,** [2,6-{Ph_2PNMe}$_2$(NC_5H_3)]CuOTf, and the HOFO's for compounds **1** and **3** display similar geometries. The energy and the orbital label for HOFO-5/HOFO-6 (i.e. HOFO-6 for **1** and HOFO-5 for **2-3**) depends on the specific compound. The table provides a summary of the percent occupancy change for each HOFO in complexes **1-3**.

The donor array presented by the ligand is nearly identical to that observed for **1** with six major HOFO donor orbitals with electron donations that was almost the same as for **1** (see data in Figure 3). The most significant difference was an increase in donation from the P-centers (HOFO) to the Cu 4p orbital. The HOFO-1 donor is also similar in shape to the analogous orbital in complex **1** and overlaps in a combination of bonding and anti-bonding interactions with the Cu 4s orbital. Due to a small shift in donor orbital energies, the orbital labeled HOFO-6 in compound **1** now bears the label HOFO-5. This orbital, essentially a lone electron pair on N_{py}, contributes even less to Cu-ligand bonding than with **1**. The HOFO-12 and HOFO-13 are approximately equal and in-phase contributions from the two P centers and the N_{py}/polarized-π orbitals. These two orbitals are of appropriate symmetry to donate to the 4s Cu orbital. Interestingly, the increase in effective charge on the Cu(I) center in **2** produced the greatest increase in donation from the ligand P centers and actually a decrease in direct donation from the N_{py} centered lone electron pair.

In the case of complex **2**, there is a significant bonding contribution due to back donation from the occupied d-orbitals of Cu(I). All five or these d-orbitals participate and have similar changes in orbital occupancy from this back donation that range from 1.1% to 3.6% change. The total change amounts to 10.7% which equates to 0.2 electrons of back donation from Cu to ligand. The acceptor orbitals on the ligand are spread over a set of orbitals that are close to each other in energy and are mostly π* in character.

The electronic analysis of **1** and **2** emphasizes that the interaction of PN^3P ligands with metal centers is a balance of bonding and antibonding interactions and can involve more diffuse polarized-π orbitals. Furthermore, back-donation can play an important role in the overall

bonding picture. Many of these features would be missed or possibly misinterpreted in the absence of computational results.

These results prompted further investigation of the application of ligand **B** to the heavy congeners in group 11. The direct reaction of [2,6-{Ph_2PNMe}$_2$(NC_5H_3)] (**B**) and AgOTf proceeded smoothly in the dark to yield colorless [2,6-{Ph_2PNMe}$_2$(NC_5H_3)]AgOTf in >85% yield (Scheme 2). The NMR spectra of **3** correlate with those observed for **1**, **2** and with literature reports and display a symmetrical set of ligand signals.[24,30] A single resonance in the $^{31}P\{^1H\}$ NMR spectrum at δ 45.9 appeared with coupling to ^{107}Ag (J = 517 Hz) and ^{109}Ag (J = 549 Hz). The ratio of these values, 1.06, is close to the relative gyromagnetic ratios of 1.15 for these nuclei. In addition, these coupling constants are similar to the reported complexes **I**[43] and **J**[41].

SCHEME 2.

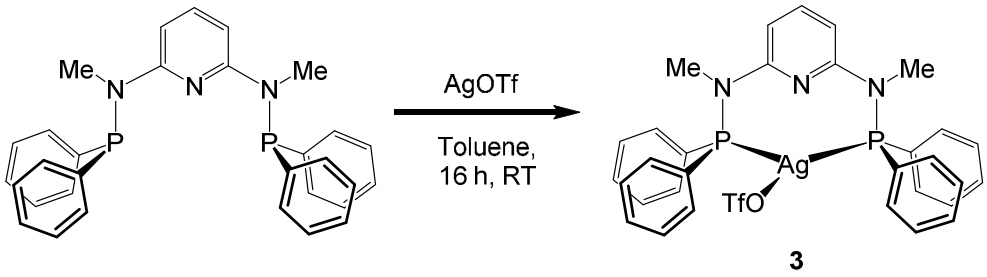

3

Crystals suitable for X-ray analysis were obtained from a saturated chloroform solution of **3** (Figure 4). In contrast to the Cu analogue, **2**, the Ag(I) center in complex **3** resides in a three coordinate environment defining a slightly pyramidalized trigonal planar geometry. In addition to the two symmetrically bonded phosphine groups from the ligand at average bond distances of 2.47Å, one of the oxygen centers of the OTf anion (Ag-O(1) 2.393(2)Å) completes the Ag coordination sphere. The sum of angles for these ligated centers has a value of 351.8º and

confirms the non-planar geometry. The Ag-N_{py} distance 2.674Å is notably beyond a more typical covalent bonding distance of 2.2-2.4Å. The literature provides a comparison to **3** from the structurally characterized cationic complex **I**[43] and the four coordinate complex **J**.[41] Compound **I** exhibited a two coordinate, non-linear Ag(I) center with Ag-P ≈ 2.40Å, a P-Ag-P angle of 157.87(2)° and a Ag···N of 2.4642(17)Å. All of these distances are shorter than in **3** as might be expected for the lower coordination number. For **J**, the Ag-P (2.5006(9), 2.5229(9)Å) and Ag-OTf (2.495(2)Å) bond lengths are only slightly longer than those found for **3** and the non-bonded nitrogen atom of the ligand in **J** is essentially the same distance from the silver atom (2.680(2) Å) as observed for **3**. A notable contrast between complexes **J** and **3** is the coordination of a fourth ligand to the Ag center in **J** leading to an $18e^-$ configuration and a distorted-tetrahedral structure.

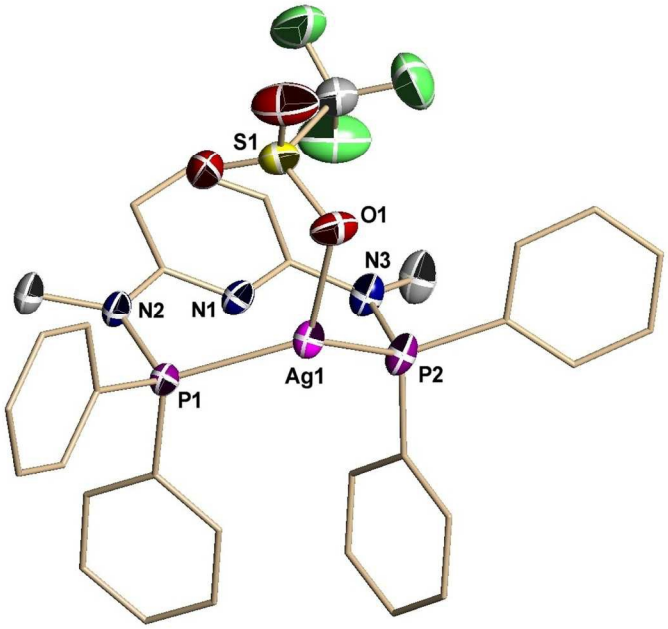

Figure 4. Structural representation of compound **3**. Hydrogen atoms and thermal ellipsoids of the ligand carbon atoms are omitted for clarity. Full structural information can be found in the Supporting Information. Selected bond lengths (Å) and bond angles (deg) Ag(1)-O(1) 2.393(2),

Ag(1)-P(2) 2.4663(7), Ag(1)-P(1) 2.4836(6), Ag(1)-N(1) 2.674, P(1)-N(3) 1.715(2), P(2)-N(2) 1.705(2), O(1)-Ag(1)-P(2) 116.50(7), O(1)-Ag(1)-P(1) 115.48(7), P(2)-Ag(1)-P(1) 119.82(2)

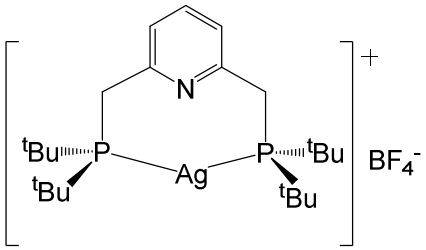

I

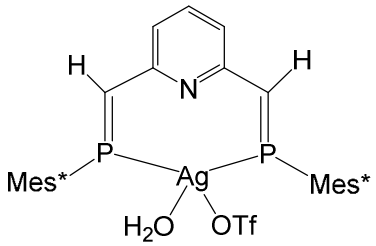

J

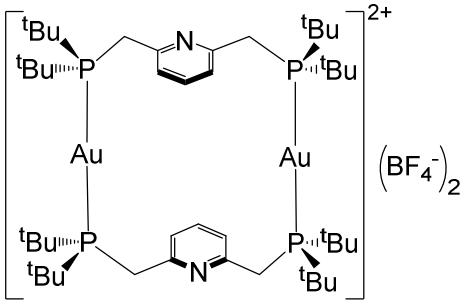

K

A DFT computational study using the B3LYP functional with the mixed DZVP/TZVP basis set was undertaken to obtain a more thorough understanding of the electronic nature of compound **3** and to allow a comparison with **1**, **2** and the reported Ag[bis(imino)pyridine]$^{+}$OTf^{-} analogues.[17,19] Optimization produced a structure that was in agreement with the X-ray structure results and the electronic interaction energy between the LAg and the OTf fragments was determined to be -82.8 kcal/mol. The bond order between these fragments was rather low at 0.26, which corresponded with donation of only 0.15 electrons from the OTf^{-} anion to the LAg^{+} fragment. These results are comparable to what was obtained for the cation/anion interaction for Ag[bis(imino)pyridine]$^{+}$OTf^{-}.

Within the [2,6-{Ph_2PNMe}$_2$(NC_5H_3)]Ag fragment, the computational results revealed an electronic interaction energy of -94.4 kcal/mol between the ligand and the Ag center which, in this case, is largely due to covalent bonding between the metal ion and the ligand. The corresponding total bond order between these fragments was determined to be 1.41 and electron donation from the ligand to the Ag(I) center of 0.82 electrons very effectively quenches the majority of the silver cation charge. As expected for the d^{10} Ag(I) fragment the four acceptor

orbitals are the 5s and 5p orbitals (LUFO and LUFO+1 to LUFO+3). The specific amount of electron density accepted by each of these orbitals varies with the most significant accepting orbital being the LUFO which changes occupancy by 25%. There is less donation (11% of the occupancy change) for LUFO+1. This overall reduced donation relative to the Cu complexes (**1** and **2**) is consistent with the increase in principle quantum number for the acceptor orbitals of Ag.

The dominant donor orbitals from the ligand fragment remain similar and are displayed in Figure 3 along with their percent occupancy change for **3**. The most significant donor is the HOFO-1, dominated by the P centers, which has a 15.4% change in orbital occupancy. Again, this orbital has a combined σ-bonding interaction from the two P centers with a σ^*-bonding interaction with the N_{py}. These results are entirely consistent with the crystallographically determined structure indicating P/Ag bonding and little or no bonding interaction between Ag and N_{py}. The remaining four ligand fragment orbitals (HOFO, HOFO-2, HOFO-12, HOFO-13) each donate approximately the same electron density to Ag^+ (Fig. 2). As observed with the Cu complexes, two of these orbitals donate to Ag 5p (HOFO and HOFO-2) and two of them (HOFO-12 and HOFO-13) have a significant component that is a polarized π-orbital that is localized on the N_{py} center. The result of these ligand/Ag^+ interactions is a symmetrical bonding with resulting Mayer bond orders for the Ag-P of 0.64 and 0.59 and for the Ag-N a value of 0.12.

Complexes of ligand **B** with the group 11 triad were completed by direct reaction of this ligand with $AuCl(SMe_2)$ at room temperature in dichloromethane. Interestingly, regardless of stoichiometry employed for this reaction, the only isolated species was the 1:2 adduct **4**, 2,6-$\{Ph_2PNMe\}_2(NC_5H_3)](AuCl)_2$ (Scheme 3).

SCHEME 3.

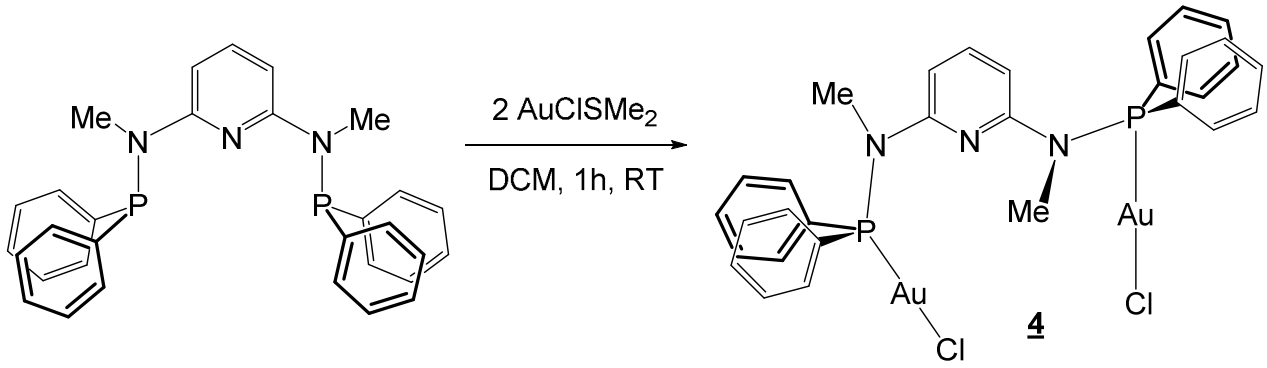

The NMR spectra for **4** were consistent with a symmetrical structure and the observation of a ^{31}P resonance at δ 67.5 ppm was similar to the analogous reported Au(I) complex of ligand **A**, 2,6-$\{Ph_2PNH\}_2(NC_5H_3)](AuCl)_2$ which exhibited a sharp singlet with chemical shift at 56.3 ppm.[35]

The structural features of **4** were confirmed by single crystal X-ray analysis (Figure 5). In contrast to the monometallic Cu and Ag complexes, compound **4** displayed a ligand that binds in a monodentate fashion through the two phosphino groups, which coordinate independently to two different Au(I) centers leading to a bimetallic species. The coordination geometry of **4** is the commonly observed linear coordination of Au(I) that is favored even when the ligand offers additional potential bonding sites as with **B**.[37] The structure of the NH analogue 2,6-$\{Ph_2PNH\}_2(NC_5H_3)](AuCl)_2$ has been reported twice.[34,35] The bonding parameters obtained for **4** are, not surprisingly, nearly identical to these structures. The reported structure, **K**,[43] with a related PNP ligand, is an interesting bimetallic species that exhibited a similar metal coordination pattern. However, in that case, it was likely the weakly coordinating behavior of the BF_4^- anion that allowed for the coordination of two ligands to each Au center leading to the formation of the

observed macrocyclic compound. In **K**, the gold center displayed a linear P-Au-P coordination (173.91(3)°) with slightly longer Au-P distances of 2.31-2.32Å.

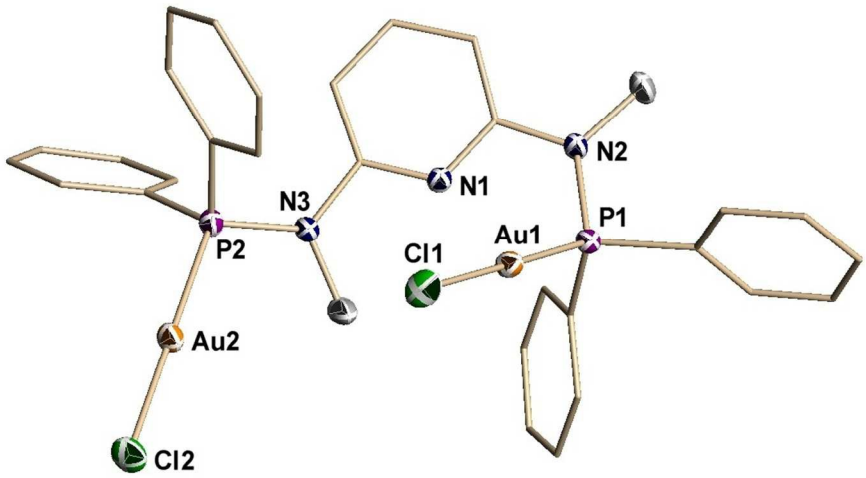

Figure 5. Structural representation of compound **4**. Hydrogen atoms and thermal ellipsoids of the ligand carbon atoms are omitted for clarity. Full structural information can be found in the Supporting Information. Selected bond lengths (Å) and bond angles (°) Au(1)-P(1) 2.2297(8), Au(1)-Cl(1) 2.2867(8), Au(2)-P(2) 2.2269(8), Au(2)-Cl(2) 2.2813(9), P(1)-N(2) 1.699(2), P(2)-N(3) 1.682(2), P(1)-Au(1)-Cl(1) 177.53(3), P(2)-Au(2)-Cl(2) 178.72(3)

Conclusion

This report provides the first family of group 11 metal complexes of the N,N'-bis(diphenylphosphino)-2,6-di(methylamino)pyridine ligand. The two Cu(I) complexes display unique molecular structures with the Cu center in a trigonal pyramidal coordination environment. This contrasts with the analogous ligand where N-Me is replaced by N-H and bidentate ligand coordination is favored. The Ag(I) complex, [2,6-{Ph_2PNMe}$_2$(NC_5H_3)]AgOTf, is the first reported silver complex of this ligand family. In this species, the ligand coordinates in a bidentate fashion through the two phosphine groups which yields a pyramidally distorted trigonal

planar silver coordination geometry. The structure for the monovalent Au compound displays a dinuclear compound in which each P center of the ligand is independently coordinated to different Au(I) centers having linear coordination geometries. This is consistent with the only other reported gold complex of this ligand family.

Electronic structure and bonding analysis provided a richer view of the versatility of this ligand for metal binding. Computations provided the general donor orbital array for the κ^3-PN^{3}P ligand and highlights the relative role of P and N bonding as well as the effects of the acceptor orbitals on metal-ligand bonding. While the donation from the P-centers is dominant and relatively straightforward, the Cu-N_{py} interaction is more subtle, involving a combination of antibonding and bonding σ interactions. In addition, N_{py} bonding interactions involve a set of polarized π-based orbitals; an interaction that is only revealed through computational analysis. As demonstrated by complex **2**, the PN^{3}P ligand can participate in significant back-donation from the occupied d-orbitals of Cu(I).

The use of ligand **B** with an N-Me versus either an N-H or CH_2 linker provides group 11 complexes that should be less susceptible to ligand deprotonation/reaction with strong bases.[38,39,44] Our continuing efforts target an expansion of our understanding of the metal/ligand interactions in these and related complexes as well as the exploitation of these effects in reactivity.

Experimental Section

General Methods. Reactions were performed in a glovebox under a nitrogen atmosphere, with the exception of ligand synthesis, which was performed using standard Schlenk techniques under

a flow of N_2. All solvents were sparged with nitrogen and then dried by passage through a column of activated alumina using an apparatus purchased from Anhydrous Engineering. Deuterated solvents were dried using activated molecular sieves. Metal starting materials were purchased from Strem Chemicals and used as received. All other chemicals were purchased from Aldrich and used without further purification. Ligand **B** was synthesized according to literature procedures.[24] NMR spectra were run on a Bruker Avance 300 MHz spectrometer using the residual protons of the NMR solvent as internal standards. Elemental analysis was performed by Midwest Microlab, LLC, Indianapolis, IN.

2,6-{Ph_2PNMe}$_2$(NC_5H_3)]CuBr (1) Copper(I) bromide dimethyl sulfide (0.081 g, 0.4 mmol) was mixed with ligand **B** (0.202 g, 0.4 mmol) in CH_2Cl_2 (10 mL) and stirred for 1 h at room temperature. The volume of solvent was reduced to 3 mL and 30 mL of hexane was added. The light green precipitate was filtered and dried in vacuo to give **1**. The crystals were grown by diffusion of hexanes into a solution of CH_2Cl_2 at room temperature in a week. Yield 0.212 g (82%). ^{1}H NMR (300 MHz, $CDCl_3$, 25°C): δ = 2.83 (s, 6H, CH_3), 6.19 (d, J = 8.1 Hz, 2H), 7.26−7.38 (m, 12H), 7.41−7.54 (m, 9H). $^{13}C\{^1H\}$ NMR (75 MHz, $CDCl_3$, 25 ºC): δ = 32.8 (CH_3), 98.5 (py), 128.5 (t, J = 4.0 Hz, Ph),130.1 (Ph), 132.1 (t, J = 11.4 Hz, Ph), 132.8 (t, J = 8.6 Hz, Ph), 141.8 (py), 156.2 (t, J = 8.3 Hz, py). $^{31}P\{^1H\}$ NMR (121 MHz, $CDCl_3$, 25 °C): δ = 45.0. HR-MS (CH_3CN): [M−Br] m/z; calcd value for $C_{31}H_{29}N_3P_2Cu$ (δ). [M−Br] m/z 568.1157; calcd value for $C_{31}H_{29}N_3P_2Cu$ 568.1133 (δ 4.3). Analysis for $C_{31}H_{29}N_3P_2BrCu$: Calculated, C 57.37, H 4.50, N 6.47, Found C 57.22, H 4.52, N 6.29.

2,6-{Ph_2PNMe}$_2$(NC_5H_3)]CuOTf (2): 2,6-{Ph_2PNMe}$_2$(NC_5H_3)]CuBr (0.129 g, 0.2 mmol) was dissolved in 10 mL of dichloromethane. A solution of AgOTf (0.051 g, 0.2 mmol) dissolved in 3 mL toluene was added drop wise to the solution of **1** and the reaction mixture was stirred for 2 h at room temperature. A white precipitate formed and was removed by filtration and solvent was dried in vacuo to give **2**. The crystals were grown by diffusion of hexanes into a solution of dichloromethane at room temperature. Yield 0.102 g (78%). ^{1}H NMR (300 MHz, CD_2Cl_2, 25°C): δ = 2.86 (s, 6H, CH_3), 6.31 (d, J = 7.0 Hz, 2H), 7.29−7.42 (m, 20H), 7.64 (t, J = 8.1 Hz, 1H). ^{13}C{^{1}H} NMR (75 MHz, CD_2Cl_2, 25 ºC): δ = 33.6 (CH_3), 99.9 (py), 129.3 (Ph), 130.6 (Ph), 131.4 (Ph), 133.1 (Ph), 143.2 (py), 156.6 (py). ^{31}P{^{1}H} NMR (121 MHz, CD_2Cl_2, 25 °C): δ = 45.5. ^{19}F{^{1}H} NMR (282 MHz, CD_2Cl_2, 25 °C): δ = −78.5. HR-MS (CH_3CN): [M−CF_3SO_3] m/z 568.1120; calcd value for $C_{31}H_{29}N_3P_2Cu$ 568.1133 (δ −2.2). ESI (negative mode) showed a peak at m/z 148.8744 which corresponded to CF_3SO_3. Analysis for $C_{32}H_{29}N_3P_2F_3O_3SCu$: Calculated, C 53.52, H 4.07, N 5.85, Found C 53.71, H 4.48, N 5.55.

2,6-{Ph_2PNMe}$_2$(NC_5H_3)]AgOTf (3) Silver trifluoromethanesulfonate (AgOTf) (0.102 g, 0.4 mmol) was added to the toluene (15 mL) solution of ligand **B** (0.202 g, 0.4 mmol). The reaction mixture was wrapped with aluminum foil and stirred for 16 h. The solution was filtered, evaporated and was washed with 10 mL hexanes. It was dry under vacuum to give **3** as colorless crystalline solid. Crystals suitable for X-ray were grown by diffusion of hexanes into a saturated $CDCl_3$ solution at room temperature. Yield 0.261 g (86%). ^{1}H NMR (400 MHz, $CDCl_3$, 25 °C): δ = 2.88 (t, J = 1.94 Hz, 6H, CH_3), 6.42 (d, J = 8.0 Hz, 2H), 7.33−7.36 (m, 8H), 7.42−7.47 (m, 12H), 7.62 (t, J = 8.0 Hz, 1H). ^{13}C{^{1}H} NMR (100 MHz, $CDCl_3$, 25 ºC): δ = 34.2 (t, J = 3.2 Hz, CH_3), 100.6 (py), 128.9 (t, J = 4.7 Hz, Ph), 130.7 (Ph), 131.6 (t, J = 12 Hz, Ph), 132.6 (t, J = 9.6

Hz, Ph), 140.8 (py), 156.6 (t, J = 6.8 Hz, py). $^{31}P\{^{1}H\}$ NMR (162 MHz, $CDCl_3$, 25 °C): δ = 45.9 (dd, J^{109}Ag-P = 549 Hz, J^{107}Ag-P = 517 Hz). HR-MS (CH_3CN): [M−OTf] m/z 612.0869; calcd value for $C_{31}H_{29}N_3P_2Ag$ 612.088 (δ –3.1). Analysis for $C_{32}H_{29}N_3P_2F_3O_3SAg$: Calculated, C 50.41, H 3.83, N 5.51, Found C 50.26, H 3.78, N 5.48.

2,6-{Ph_2PNMe}$_2$(NC_5H_3)]($AuCl)_2$ (4) Chloro(dimethylsulfide)gold(I) (0.118 g, 0.4 mmol) was added to the CH_2Cl_2 (10 mL) solution of ligand **B** (0.202 g, 0.2 mmol). The reaction mixture was stirred for 1h. After filtration, the solution was concentrated to 2 ml, and reprecipitated with hexane to give colorless compound **4**. The crystals suitable for X-ray were grown by slow diffusion of hexane to the CH_2Cl_2 solution of **3**. Yield 0.154 g (80%). ^{1}H NMR (300 MHz, CD_2Cl_2, 25 °C): δ = 2.73 (s, 3H, CH_3), 2.75 (s, 3H, CH_3), 6.81 (d, J = 8.0 Hz, 2H), 7.53−7.67 (m, 21H). $^{13}C\{^{1}H\}$ NMR (75 MHz, CD_2Cl_2, 25 ºC): δ = 36.0 (s, CH_3), 105.6 (d, J = 6.4 Hz, py), 129.5 (d, J = 12.3 Hz, Ph), 130.8 (d, J = 66.7 Hz, Ph), 132.4 (d, J = 2.3 Hz, Ph), 133.2 (d, J = 15.7 Hz, Ph), 139.6 (py), 156.2 (d, J = 8.9 Hz, py). $^{31}P\{^{1}H\}$ NMR (121 MHz, CD_2Cl_2, 25 °C): δ = 67.5. HR-MS (CH_3CN): [M−$AuCl_2$] m/z 702.1535; calcd value for $C_{31}H_{29}N_3P_2Au$ 702.1502 (δ 4.7). Analysis for $C_{31}H_{29}N_3P_2Cl_2Au_2$: Calculated, C 38.37, H 3.01, N 4.33, Found C 38.09, H 3.10, N 4.12.

X-ray Crystallography

Data collection results for compounds **1-4** represent the best data sets obtained in several trials for each sample. The crystals were mounted on thin glass fibers using paraffin oil. Prior to data collection crystals were cooled to 200.15 °K. Data were collected on a Bruker AXS SMART single crystal diffractometer equipped with a sealed Mo tube source (wavelength 0.71073 Å)

APEX II CCD detector. Raw data collection and processing were performed with APEX II software package from BRUKER AXS.[45] Initial unit cell parameters were determined from 60 data frames with 0.3° ω scan each collected at the different sections of the Ewald sphere. Semi-empirical absorption corrections based on equivalent reflections were applied.[46] Systematic absences in the diffraction data-set and unit-cell parameters were consistent with triclinic $P\bar{1}$ (№2) for compounds **1-3**, and orthorhombic $P2_1/c$ for compound **4**. The structures were solved by direct methods, completed with difference Fourier synthesis, and refined with full-matrix least-squares procedures based on F^2.

For all the compounds all hydrogen atoms positions were calculated based on the geometry of the related non-hydrogen atoms. All hydrogen atoms were treated as idealized contributions during the refinement. All scattering factors are contained in several versions of the SHELXTL program library, with the latest version used being v.6.12.[47]

Computational Details

Density functional theory (DFT) calculations have been performed using the Gaussian 09 package.[48] The structures of all species were optimized using the B3LYP exchange-correlation functionals with the DZVP basis set and effective-core potential for Ag and the all-electron TZVP basis set for all other elements unless indicated otherwise. Tight SCF convergence criteria (10^{-8} a.u.) were used for all calculations.

The analysis of the molecular orbital (MO) compositions in terms of occupied and unoccupied orbitals of the fragment species (HOFOs and LUFOs, respectively) was performed, and Mayer bond orders were calculated using the AOMix program.[49,50] Atomic charges were evaluated by using the natural population analysis (NPA).

REFERENCES

1 H. A. Younus, W. Su, N. Ahmad, S. Chen and F. Verpoort, *Adv. Synth. Catal.*, 2015, **357**, 283–330.

2 D. Milstein, *Phil. Trans. R. Soc. A*, 2015, **373**, 20140189.

3 C. Gunanathan and D. Milstein, *Chem. Rev.*, 2014, **114**, 12024–12087.

4 D. M. Roddick and D. Zargarian, *Inorganica Chim. Acta*, 2014, **422**, 251–264.

5 H. Li, B. Zheng and K.-W. Huang, *Coord. Chem. Rev.*, 2015, **293-294**, 116–138.

6 C. Gunanathan and D. Milstein, *Science*, 2013, **341**, 1229712.

7 J. Choi, A. H. R. MacArthur, M. Brookhart and A. S. Goldman, *Chem. Rev.*, 2011, **111**, 1761–1779.

8 N. Selander and K. J. Szabó, *Chem. Rev.*, 2011, **111**, 2048–2076.

9 S. Schneider, J. Meiners and B. Askevold, *Eur. J. Inorg. Chem.*, 2012, 412–429.

10 J. I. Van Der Vlugt and J. N. H. Reek, *Angew. Chemie - Int. Ed.*, 2009, **48**, 8832–8846.

11 L. C. Liang, *Coord. Chem. Rev.*, 2006, **250**, 1152–1177.

12 M. E. van der Boom and D. Milstein, *Chem. Rev.*, 2003, **103**, 1759–1792.

13 M. Albrecht and M. M. Lindner, *Dalton Trans.*, 2011, **40**, 8733–8744.

14 T. Jurca, L. K. Hiscock, I. Korobkov, C. N. Rowley and D. S. Richeson, *Dalton Trans.*, 2014, **43**, 690–7.

15 T. Jurca, I. Korobkov, S. I. Gorelsky and D. S. Richeson, *Inorg. Chem.*, 2013, **52**, 5749–5756.

16 T. Jurca, J. Lummiss, T. J. Burchell, S. I. Gorelsky and D. S. Richeson, *J. Am. Chem. Soc.*, 2009, **131**, 4608–4609.

17 T. Jurca, S. Ouanounou, S. I. Gorelsky, I. Korobkov and D. S. Richeson, *Dalton Trans.*, 2012, **41**, 4765.

18 T. Jurca, I. Korobkov, G. P. a Yap, S. I. Gorelsky and D. S. Richeson, *Inorg. Chem.*, 2010, **49**, 10635–10641.

19 T. Jurca, S. I. Gorelsky, I. Korobkov and D. S. Richeson, *Dalton Trans.*, 2011, **40**, 4394–4396.

20 T. Jurca, A. Farghal, P. Lin, I. Korobkov, M. Murugesu and D. S. Richeson, *J. Am. Chem. Soc.*, 2011, **133**, 15814–15817.

21 W. Schirmer, U. Florke and H.-J. Haupt, *Z. Anorg. Allg. Chem.*, 1987, **545**, 83–97.

22 W. Schirmer, U. Florke and H.-J. Haupt, *Z. Anorg. Allg. Chem.*, 1989, **574**, 239–255.

23 U. Florke and H.-J. Haupt, *Zeitschrift fur Crystallogr.*, 1991, **196**, 299.

24 S. R. M. M. De Aguiar, B. Stöger, E. Pittenauer, M. Puchberger, G. Allmaier, L. F. Veiros and K. Kirchner, *J. Organomet. Chem.*, 2014, **760**, 74–83.

25 B. Bichler, C. Holzhacker, B. Stöger, M. Puchberger, L. F. Veiros and K. Kirchner, *Organometallics*, 2013, **32**, 4114–4121.

26 Ö. Öztopcu, C. Holzhacker, M. Puchberger, M. Weil, K. Mereiter, L. F. Veiros and K. Kirchner, *Organometallics*, 2013, **32**, 3042–3052.

27 D. Benito-Garagorri, L. G. Alves, L. F. Veiros, C. M. Standfest-Hauser, S. Tanaka, K. Mereiter and K. Kirchner, *Organometallics*, 2010, **29**, 4932–4942.

28 D. Benito-Garagorri, L. G. Alves, M. Puchberger, K. Mereiter, L. F. Veiros, M. J. Calhorda, M. D. Carvalho, L. P. Ferreira, M. Godinho and K. Kirchner, *Organometallics*, 2009, **28**, 6902–6914.

29 D. Benito-Garagorri, J. Wiedermann, M. Pollak, K. Mereiter and K. Kirchner, *Organometallics*, 2007, **26**, 217–222.

30 D. Benito-Garagorri, E. Becker, J. Wiedermann, W. Lackner, M. Pollak, K. Mereiter, J. Kisala and K. Kirchner, *Organometallics*, 2006, **25**, 1900–1913.

31 S. Qu, Y. Dang, C. Song, M. Wen, K. W. Huang and Z. X. Wang, *J. Am. Chem. Soc.*, 2014, **136**, 4974–4991.

32 L. P. He, T. Chen, D. X. Xue, M. Eddaoudi and K. W. Huang, *J. Organomet. Chem.*, 2012, **700**, 202–206.

33 H. A. Younus, N. Ahmad, W. Su and F. Verpoort, *Coord. Chem. Rev.*, 2014, **276**, 112–152.

34 N. Biricik, Z. Fei, R. Scopelliti and P. J. Dyson, *Eur. J. Inorg. Chem.*, 2004, 4232–4236.

35 Z. Pan, M. T. Gamer and P. W. Roesky, *Z. Anorg. Allg. Chem.*, 2006, **632**, 744–748.

36 L. Yang, D. R. Powell and R. P. Houser, *Dalton Trans.*, 2007, 955–964.

37 M. A. Carvajal, J. J. Novoa and S. Alvarez, *J. Am. Chem. Soc.*, 2004, **126**, 1465–1477.

38 J. I. Van Der Vlugt, E. A. Pidko, D. Vogt, M. Lutz and A. L. Spek, *Inorg. Chem.*, 2009, **48**, 7513–7515.

39 J. I. Van Der Vlugt, E. A. Pidko, D. Vogt, M. Lutz, A. L. Spek and A. Meetsma, *Inorg. Chem.*, 2008, **47**, 4442–4444.

40 J. I. Van Der Vlugt, E. A. Pidko, R. C. Bauer, Y. Gloaguen, M. K. Rong and M. Lutz, *Chem. Eur. J.*, 2011, **17**, 3850–3854.

41 A. Hayashi, M. Okazaki and F. Ozawa, *Organometallics*, 2007, **26**, 5246–5249.

42 C. Müller, E. A. Pidko, M. Lutz and A. L. Spek, *Chem. - A Eur. J.*, 2008, **14**, 8803–8807.

43 J. I. Van Der Vlugt, M. a. Siegler, M. Janssen, D. Vogt and A. L. Spek, *Organometallics*, 2009, **28**, 7025–7032.

44 S. Y. De Boer, Y. Gloaguen, M. Lutz and J. I. Van Der Vlugt, *Inorg. Chim. Acta*, 2012, **380**, 336–342.

45 APEX Softward Suite v 2010; Bruker AXS: Madison WI.

46 B. Y. R. H. Blessing, *Acta Crystallogr. Sect. A*, 1995, 33–38.

47 G. M. Sheldrick, *Acta Crystallogr. Sect. A*, 2008, 112–122.

48 M. J. Frisch, G. W. Trucks, H. B. Schlegel, G. E. Scuseria, M. A. Robb, J. R. Cheeseman, G. Scalmani, V. Barone, B. Mennucci, G. A. Petersson, H. Nakatsuji, M. Caricato, X. Li, H. P. Hratchian, A. F. Izmaylov, J. Bloino, G. Zheng and D. J. Sonnenb, Gaussian 09, Revision A.02.

49 S. I. Gorelsky, AOMix software for molecular orbital analysis. Version 6.8 2013.

50 S. I. Gorelsky and A. B. P. Lever, *J. Organomet. Chem.*, 2001, **635**, 187–196.

TOC figure

Coinage Metal Complexes of a Neutral Pincer Ligand with a “PN3P” Scaffold.

Gyandshwar Kumar Rao, Serge Gorelksy, Ilia Korobkov, Darrin Richeson*.